geosciences

MDPI

Article

Evidences for Paleo-Gas Hydrate Occurrence: What We Can Infer for the Miocene of the Northern Apennines (Italy)

Claudio Argentino, Stefano Conti, Chiara Fioroni and Daniela Fontana *

Department of Chemical and Geological Sciences, University of Modena and Reggio Emilia, 41125 Modena, Italy; claudio.argentino@unimore.it (C.A.); stefano.conti@unimore.it (S.C.); chiara.fioroni@unimore.it (C.F.)

* Correspondence: daniela.fontana@unimore.it

Received: 25 February 2019; Accepted: 15 March 2019; Published: 20 March 2019

Abstract: The occurrence of seep-carbonates associated with shallow gas hydrates is increasingly documented in modern continental margins but in fossil sediments the recognition of gas hydrates is still challenging for the lack of unequivocal proxies. Here, we combined multiple field and geochemical indicators for paleo-gas hydrate occurrence based on present-day analogues to investigate fossil seeps located in the northern Apennines. We recognized clathrite-like structures such as thin-layered, spongy and vuggy textures and microbreccias. Non-gravitational cementation fabrics and pinch-out terminations in cavities within the seep-carbonate deposits are ascribed to irregularly oriented dissociation of gas hydrates. Additional evidences for paleo-gas hydrates are provided by the large dimensions of seep-carbonate masses and by the association with sedimentary instability in the host sediments. We report heavy oxygen isotopic values in the examined seep-carbonates up to +6‰ that are indicative of a contribution of isotopically heavier fluids released by gas hydrate decomposition. The calculation of the stability field of methane hydrates for the northern Apennine wedge-foredeep system during the Miocene indicated the potential occurrence of shallow gas hydrates in the upper few tens of meters of sedimentary column.

Keywords: gas hydrates; seep-carbonates; clathrites; Miocene; northern Apennines

1. Introduction

The sensitivity of gas hydrates to climate changes and tectonic activity is still poorly constrained and more efforts are needed to understand how they respond to these forcing processes [1–4]. In the last decades, much work has been done in terms of monitoring and modelling the gas hydrate dynamics. The investigation of seepage activities and bottom simulating reflectors (BSR) has provided quantitative results that improved the accuracy of existing models [5].

Gas hydrates are widely distributed in present-day continental margins and their stability depends on temperature, pressure and availability of gas and water [6–8]. Gas hydrates continuously dissociate and recrystallize in order to maintain their position in the sedimentary column within the stability field. When gas hydrates cannot keep pace with sedimentation and burial, they no longer fall in the stability zone and their destabilization causes the rapid release of huge amounts of fluids that induces mud diapirism, soft-sediment deformation and seafloor collapses or may trigger large-scale continental slope instability (i.e., slumps, slides) [9–13]. Shallow gas hydrates are generally associated with authigenic ^{13}C-depleted carbonates [14,15]. Gas hydrate-associated carbonates, called clathrites [16], have been sampled from present-day seafloor or a few meters below [17–23]. These carbonates may form bodies of remarkable dimension and show peculiar structures such as vacuolar or vuggy-like fabrics, association of pure aragonitic and gas hydrate layers (zebra-like structures) and breccias

produced by the destabilization of gas hydrates [18,24–26]. Geochemical indicators in porewaters (i.e., chlorine anomalies, oxygen isotopes) are also used to identify and quantify gas hydrate distribution and formation/destabilization processes [27–30]. Gas hydrate decomposition releases methane and fresh water into porewaters (low chlorine content) generating a ^{18}O-enriched signature [18,27,31–33]. Formation of gas hydrates produces enrichments in dissolved chloride content and depleted δ^{18}O values [27]. Peculiar minerals (greigite, pyrrhotite) [34,35] are also reported as possible markers of gas hydrate dissociation and their identification in the marine sedimentary record may allow the recognition of paleo-gas hydrate occurrence.

Compared to the abundant literature on present-day gas hydrates, only few studies deal with their past occurrence [36–38] or with fossil seep-carbonates recording the dissociation of gas hydrates [39–46]. In fossil sediments, the paleo-occurrence of gas hydrates is particularly challenging to assess, due to the lack of well-established proxies and to the uncertainties on the reconstruction of paleoenvironmental conditions (pressure, temperature, depth) controlling the hydrate stability field. Clathrite-like structures have been reported in fossil deposits and can be used as an indication of past gas hydrate destabilization [47,48]. Additional evidences can be yielded by geochemical signatures, the large dimensions of seep-carbonate deposits (several hundred meters in lateral extent and tens of meters in thickness) and the association with sedimentary instability (soft-sediment deformations) in hosting sediments [49].

Several Miocene seep-carbonate outcrops in different geological settings of the northern Apennines [50,51] (Figure 1) show characters suggesting paleo-gas hydrate occurrence. In this paper, we report new data and the results of twenty years of studies on seep-carbonates, obtained from field-work, facies analysis, geochemistry and biostratigraphy in order to support this hypothesis. The concentration of gas hydrate-associated carbonates in specific interval of the Miocene and their relationships with soft-sediment deformations may contribute to the understanding of factors that lead to their destabilization. Moreover, the investigation of paleo-gas hydrate in the sedimentary record may shed light into their long-term evolution and the interplay with sea level changes and tectonics [45,51].

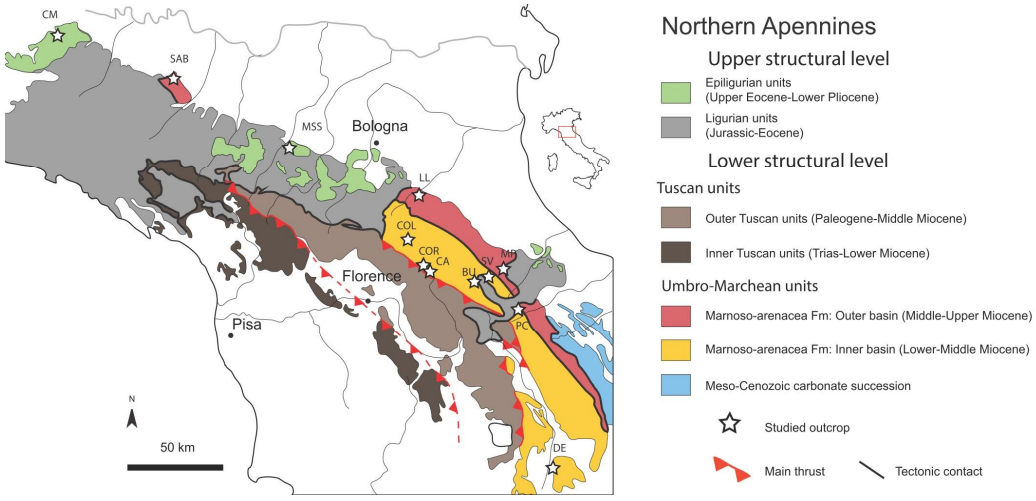

Figure 1. Simplified geological map of the northern Apennines (Italy) showing the main structural units and the location of the studied outcrops: CM = Cappella Moma [44°56′19.7″ N; 9°04′54.7″ E], SAB = Salsomaggiore [44°44′22.8″ N; 10°04′56.5″ E], MSS = Montardone, Sasso Streghe [44°28′40.3″ N; 10°47′40.7″ E], LL = Lame, Rontana [44°14′08.3″ N; 11°42′57.0″ E], COL = Colline, Mondera [44°06′41.6″ N; 11°34′22.8″ E], COR = Corella, Casellino [43°56′59″ N, 1134′59.8″ E], CA = Castagno d′Andrea [43°53′15.1″ N; 11°40′32.6″ E], MP = Montepetra [43°55′50.3″ N; 12°11′38.2″ E], SV = San Vernicio [43°54′58.4″ N; 11°57′58.3″ E], BU = Case Buscarelle [43°54′50.6″ N; 11°55′30.4″ E], PC = Poggio Campane [44°43′52.0″ N; 12°14′18.9″ E], DE = Deruta [42°58′33.3″ N; 12°26′21.1″ E].

2. Geological Setting

2.1. The Northern Apennines

The northern Apennine chain is an orogenic, NE-verging wedge, characterized by the stacking of several structural units of oceanic and continental origin (Figure 1). The complex structure of the chain is the result of the convergence and collision between the European and Africa plates, with the interposition of Adria and Corsica-Sardinia microplates. The collisional stage is accomplished by the subduction of the Adria under the Corsica-Sardinia lithosphere, coupled with the flexuring of the foreland and the formation of foredeep basins, progressively migrating towards NE [52]. The oceanic units (Ligurian units, Jurassic to Eocene), deposited within the Piedmont-Ligurian Ocean, a portion of the Tethys, comprehend a complex assemblage of highly deformed deep-marine sediments. The Epiligurian units represent the filling of wedge-top basins and are characterized by basinal to shelfal deposits (Eocene-Lower Pliocene) [52]. Ligurian and Epiligurian units represent the uppermost portion of the chain. They overlay the deformed Tuscan and Umbro-Marchean units (Figure 1) deposited on the Adria microplate and mainly consist of Mesozoic to Paleogene carbonate successions folded and segmented by thrusts (Figure 1). Foredeep basins are filled by sheet-like turbidites (Marnoso arenacea Fm); the depocenter of the basin migrated in response to the advancing Apenninic accretionary wedge incorporating the previously formed foredeep deposits. During the outward migration, the development of intrabasinal highs (Figure 2), related to blind faults and thrusts, caused the fragmentation of the foredeep into an inner and outer part [53,54]. Sedimentation on top of intrabasinal highs was mainly represented by hemipelagites and diluted turbidites (drape mudstones) forming some hundred metre thick fine-grained intervals. These structural highs represent favourable conditions to gas hydrate accumulation, seepage phenomena and sediment instability along their flanks; their deactivation heralds the successive involvement of the inner foredeep in the accretionary wedge linked to the uplift and the closure of the foredeep. During this phase, the foredeep turbidites are covered by slope marls representing the closure facies [55]: Vicchio Marls, Verghereto Marls, Ghioli di letto Fm (Figure 2) (in Figure 1, slope marls are included in Tuscan and Umbro-Marchean units). Slope marls are characterized by abundant slumps and extra formational slides, sourced by previously accreted units.

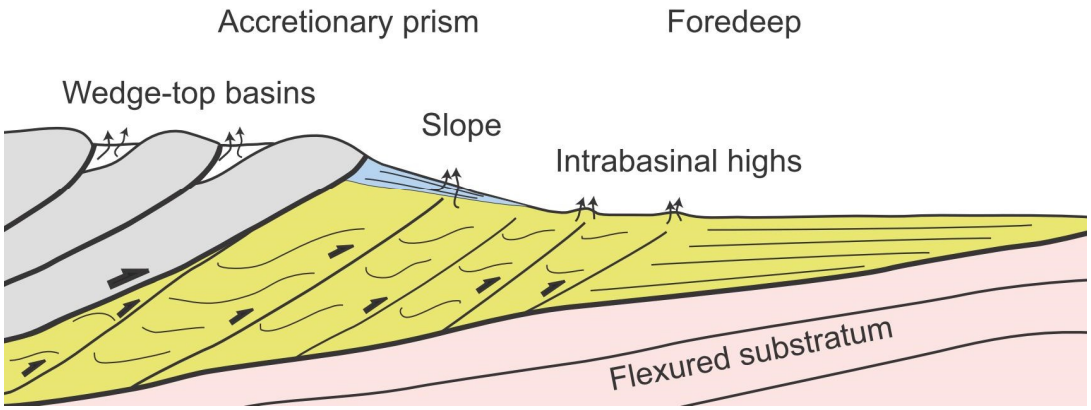

Figure 2. Schematic profile showing the main structural elements of the northern Apennine wedge-foredeep system hosting hydrate-related seep-carbonates during the Miocene: wedge-top basins (Epiligurian units, white colour) developed on top of allochthonous units (Ligurian units, grey colour), slope sediments (closure facies, light blue colour) and foredeep basin (Umbro-Marchean units, yellow colour). Intrabasinal highs developed in the inner sector of the foredeep. The position of methane seeps on the seafloor is here indicated by black arrows.

2.2. Miocene Seep-Carbonates

Large seep-carbonate bodies occur in three different positions of the Apennine wedge-top-foredeep system, from the inner to the outer setting (Figures 1 and 2):

(1) In wedge-top basins within the Epiligurian succession. The largest number of seep-carbonate bodies is within a 50 meters-thick interval in the basal portion of slope marls of the Termina Fm. The widest carbonates bodies are distributed in the peripheral portion of chaotic deposits (Montardone melange) interpreted as mud diapir [49].

(2) Along the outer slope of the accretionary prism, close to the front of the orogenic wedge. Seep-carbonates are hosted in fine-grained sediments draping thrust-bounded folds and buried ridges constituted by the older accreted turbiditic units [51]. Slope sediments including seep-carbonates have a wide extent up to 100 km parallel to the structural trend of the chain and mark the closure stage of the foredeep before the overriding of Ligurian units.

(3) At the leading edge of the deformational front in the inner foredeep, in fault-related anticlines, standing above the adjacent deep seafloor forming intrabasinal highs. Seep-carbonates are hosted in fine-grained intervals sedimented above these structures surrounded by basinal turbidites [51]. The ridges extend laterally for 10–15 km. Thrust faults are connected to the basal detachment through growing splay faults.

3. Methods

We applied different proxies to identify the occurrence of paleo-gas hydrates in the northern Apennines. It is worth mentioning that none of them is conclusively decisive when considered alone but integrated with others allow more accurate interpretations [56]. Based on a detailed field-work (Table 1), we determined number and dimension of seep-carbonate bodies in primary position (not reworked) and considered only larger outcrops, up to 1000 m of lateral extension, made up of several carbonate bodies, laterally and vertically repeated. In each outcrop we analysed larger bodies with lateral extension wider than 10 m and thickness higher than 5 m (Table 1). A detailed facies analysis allowed us to identify distinctive seep-carbonate facies and structures (breccias, non-systematic fractures, spongy fabric, drusy-like structures) referable to clathrites, described in present day settings [18,25,27]. We report the carbon and oxygen isotopic composition of Apennine seep-carbonates (new data and previous papers, Table 1, Supplementary Materials S1). We investigated the spatial and stratigraphic relationships between seep-carbonates and sedimentary instability structures related to fluid expulsion processes, such as mud volcanoes and diapirs, neptunian dikes, soft-sediment deformations, slide block, chaotic and mass transport deposits cemented by depleted micrites. The nannofossil biostratigraphy of host sediments allowed us to constrain the age of the stratigraphic interval containing seep-carbonates. We analysed outcrops that do not show any evidences of reworking. Smear slides from unprocessed sediment were prepared and analysed under a polarising light microscope at a magnification of 1250X. A semiquantitative analysis was performed for each sample by observing 100 fields of view in random traverses. In Table 1 we also included age data from previous papers [50,57]. Petrographic observations on thin sections were conducted using an optical microscope in order to identify the main carbonate phases and microfacies. Stable carbon and oxygen isotopic analyses were conducted on matrix micrite and on calcite cements filling veins and cavities. Carbonate phases were isolated by microdrilling in thin-section counterparts. Analyses were carried out at the ISO4 Stable Isotope Laboratory of the University of Turin, using a Finnigan MAT 251 mass spectrometer (Thermo Electron Corp., Waltham, MA, USA). Data are reported as range of values in ‰ notation relative to VPDB. Analytical error was better than 0.1‰ for both carbon and oxygen. Full isotopic data are reported in Supplementary Materials S1.

Table 1. Field and geochemical data of the examined seep-carbonate outcrops.

Outcrop	Geosetting	Dimension (Length × Thickness)		Samples (n)	^{13}C (‰V-PDB)	^{18}O (‰V-PDB)	Clathrite Facies	SSD	References
		Outcrop	MDAC						
MSS	Wedge-top	400 × 70	10–250 × 5–30	16	−39.1 to −18.2	+0.3 to +5.5	X	X	[49]
CM		n.m.	35 × 25	7	−30.0 to −11.0	+1.1 to +2.9	X	n.o.	[49]
SV	Slope	200 × 40	10–70 × 5–20	11	−33.2 to −27.2	+0.1 to +3.6	X	X	This work, [58]
BU		n.m.	50 × 15	2	−36.4 to −35.1	−0.3 to +1.5	X	n.o.	This work
PC		70 × 30	10–20 × 5–8	1	−32.2	+2.2	X	X	This work
SAB		250 × 35	10–25 × 5–8	18	−41.4 to −8.7	+0.2 to + 2.9	X	X	[59]
MP		100–150	10–40 × 5–10	20	−52.7 to −19,1	+0.7 to +6.0	X	X	[53]
LL		350 × 40	10–150 × 5–30	18	−51,7 to −27.4	−1.6 to + 5.0	X	n.o.	[58]
COR	Intrabasinal highs	1000 × 50	20–300 × 10–25	16	−42.3 to −26.6	−5.7 to +1.2	X	X	[51]
CA		90 × 50	12–30 × –5–10	30	−41.3 to −15.0	+0.9 to +1.2	X	X	[60]
COL		100 × 30	5–10 × 2–5	7	−56.2 to −38.9	+0.6 to +3.5	X	n.o.	This work
DE		150 × 40	10–80 × 5–20	14	−46.0 to −11.0	−4.7 to +2.2	X	X	[61]

Dimensions are reported in meters. SSD, soft-sediment deformation; n.m., not measured; n.o., not observed. Biostratigraphic data for each outcrop are reported in Section 4.1.

4. Results

We report the results from field-work, facies analysis, petrography, geochemistry and biostratigraphy of 12 seep-carbonate outcrops of the northern Apennines that show the peculiar features (i.e., dimensions, clathrite-like structures, δ^{18}O isotope and sediment instability in enclosing sediments) suggesting relationships with gas hydrates.

Seep-carbonate dimensions—The examined carbonates mainly consist of large lenticular stratiform or pinnacle-like bodies, from 10 to 300 m wide and 8 to 30 m thick (Table 1). They are arranged in horizons that extend for 700–1000 m conformable with the stratification of the enclosing fine-grained turbidites and hemipelagites. Carbonate bodies are vertically repeated and seep-impacted sediment can reach 150 m in thickness (MP outcrop).

Clathrite-like structures—Examined seep-carbonates show peculiar structures (Figure 3) such as thin layered structures consisting of an alternation of micrite and sparry calcite (Figure 3a), radial pattern of fractures (Figure 3b), spongy and vuggy-like fabrics resembling drusy crystals similar to those reported in present-day gas hydrate-associated carbonates (Figure 3c,d). Cavities are irregular in shape, circular to ellipsoidal in cross-section, empty or filled with carbonate cements and/or coarser sediments (calcarenites, peloidal sediments, microbreccias, coquina debris). They resemble voids previously occupied by solid substances (gas hydrates) that successively disappeared. The examination of cavities in thin section has allowed the identification of non-gravitational cementation fabrics and pinch-out terminations (Figure 4), ascribable to irregularly oriented dissociation of gas hydrates as proposed by [48,62] for fossil deposits in the Tertiary Piedmont Basin (north-western Apennines).

Clathrite-like structures also include fluid-induced breccias (Figure 5a–c). Monogenic and polygenic breccias are abundant, generally restricted but not exclusive, to the basal portion of carbonate bodies. Monogenic breccias are constituted by heterometric angular clasts, ranging in size from few millimetres to 5–10 cm, composed of the authigenic micrite from the seep-carbonates. Clasts are chaotically dispersed in a micritic matrix or in a fine to medium-grained sandy matrix. Larger clasts derive from the coalescence of heterometric smaller clasts, testifying various cycles of cementation and fragmentation. In many cases, monogenic breccias pass gradually to a dense and intricate network of non-systematic carbonate-filled veins and microfractures, irregularly connected to a larger vein network and conduits (Figure 5d). Polygenic breccias contain carbonate, arenitic and pelitic clasts of various stratigraphic provenance and dimensions, floating in the micritic matrix. Clasts are heterometric (from some millimetres to 50 cm in diameter), with sharp edges; clast size decreases from the base to the top of carbonate bodies. Polygenic breccias form units ranging in thickness from centimetres to a few meters, often interdigitated with fine-grained carbonate cemented sediments.

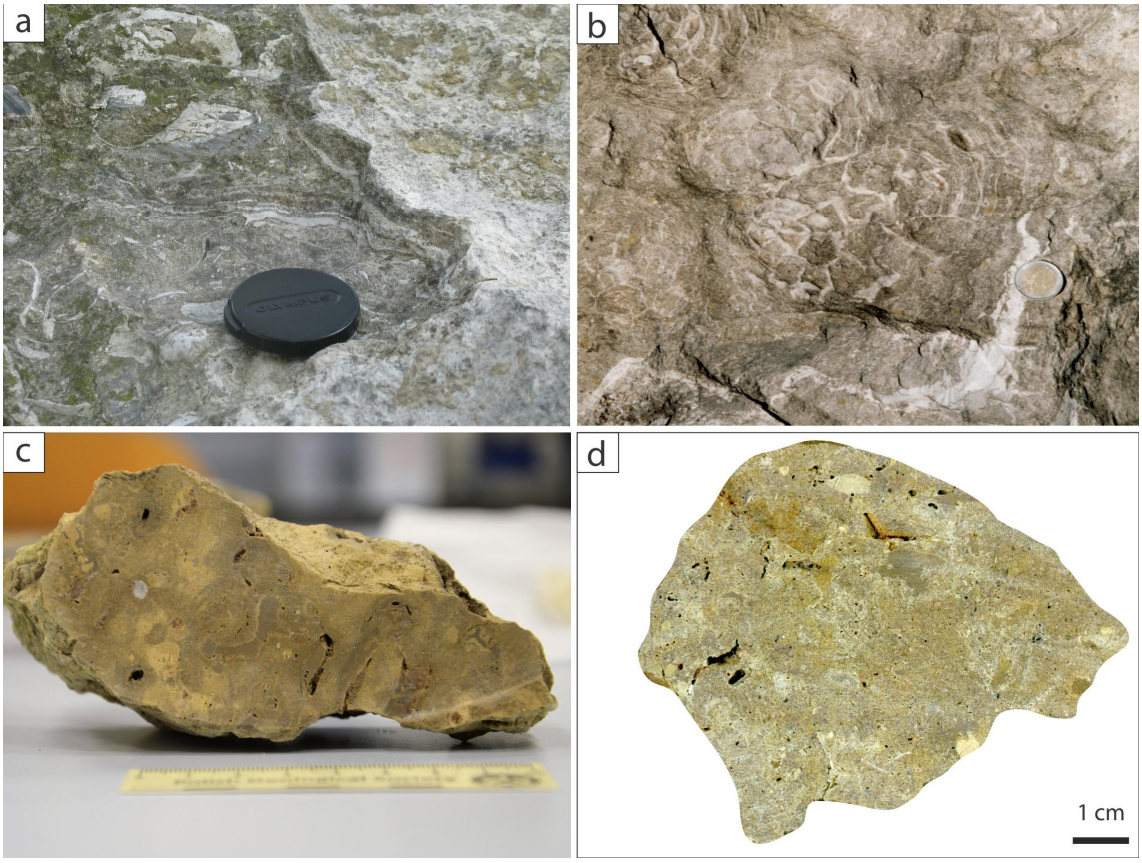

Figure 3. Examples of various clathrite-like structures. (**a**) Thin layered structures surrounding a carbonate breccia with shell fragments (MP outcrop in Figure 1). (**b**) Irregular network (mainly radial to concentric) of carbonate-filled veins (DE outcrop in Figure 1). (**c**,**d**) Vacuolar, spongy and vuggy-like fabrics: cavities have various shape, empty or filled with carbonate cements and/or coarser sediments and coquina debris. PC outcrop (**c**) and SS outcrop (**d**) of Figure 1.

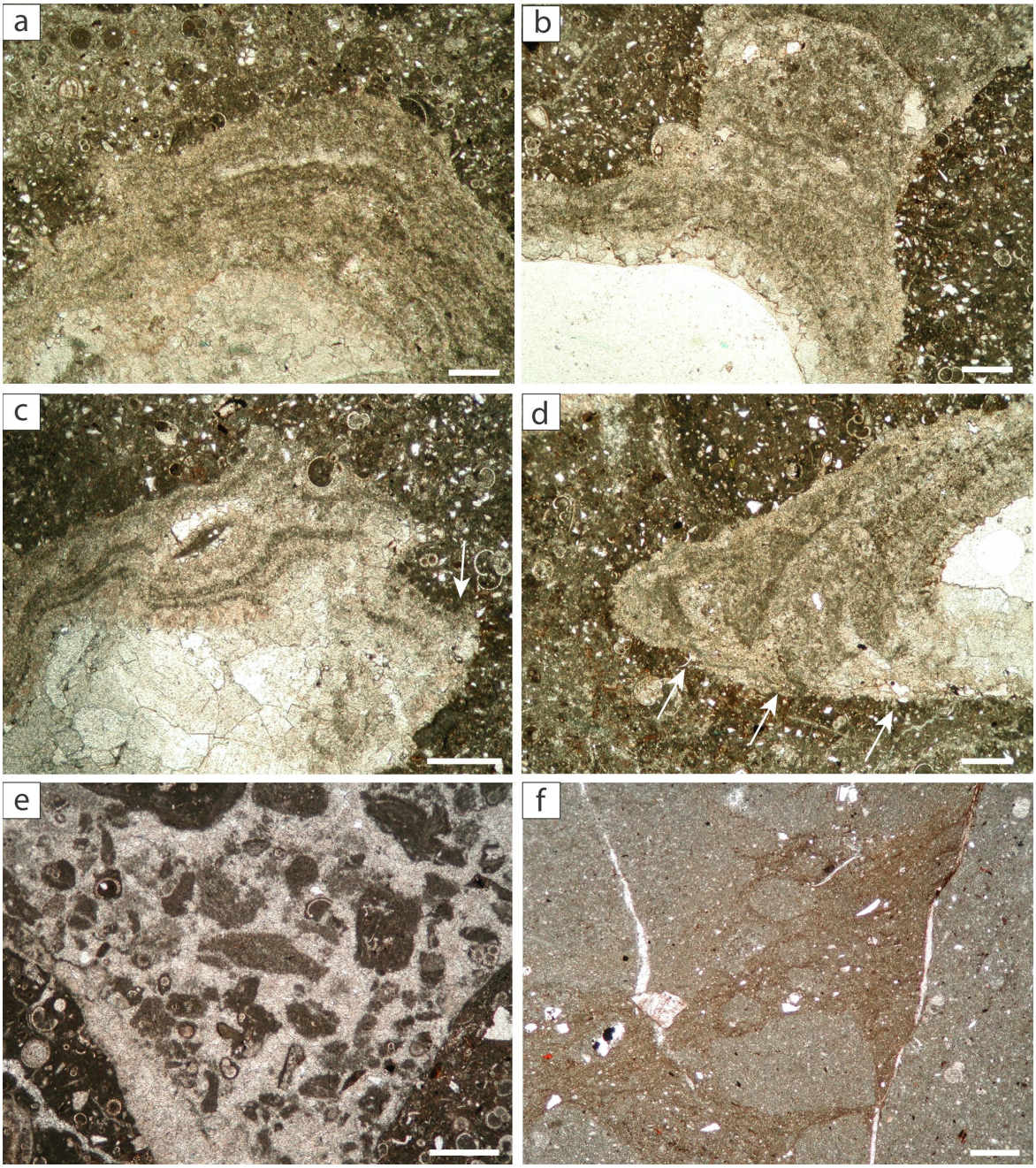

Figure 4. Micrographs displaying cavity infillings in the vuggy carbonate facies (**a**–**d**) and microbreccias (**e**,**f**). (**a**,**b**) Alternating laminae of microspatite and micrite. The thickness of the laminae varies from few microns to tens of microns. (**b**) Voids can be connected by conduits showing laminated fabric. Laminae do not line all the cavity wall but stop abruptly, in some cases producing pinch out terminations (white arrows; **c**,**d**). Calcite cements and laminae may include some tests of foraminifera or siliciclastic grains, indicating precipitation in an early diagenetic stage within semi-consolidated material. (**e**) Microbreccias composed by very angular and poorly sorted micritic clasts indicative of autoclastic fragmentation; clasts are floating in microsparitic cement. (**f**) Matrix-supported microbreccias composed by subangular clasts of micrite; clasts seem to fit to each other. Thin sections from samples of PC and COR outcrops of Figure 1. Scale bar = 1 mm.

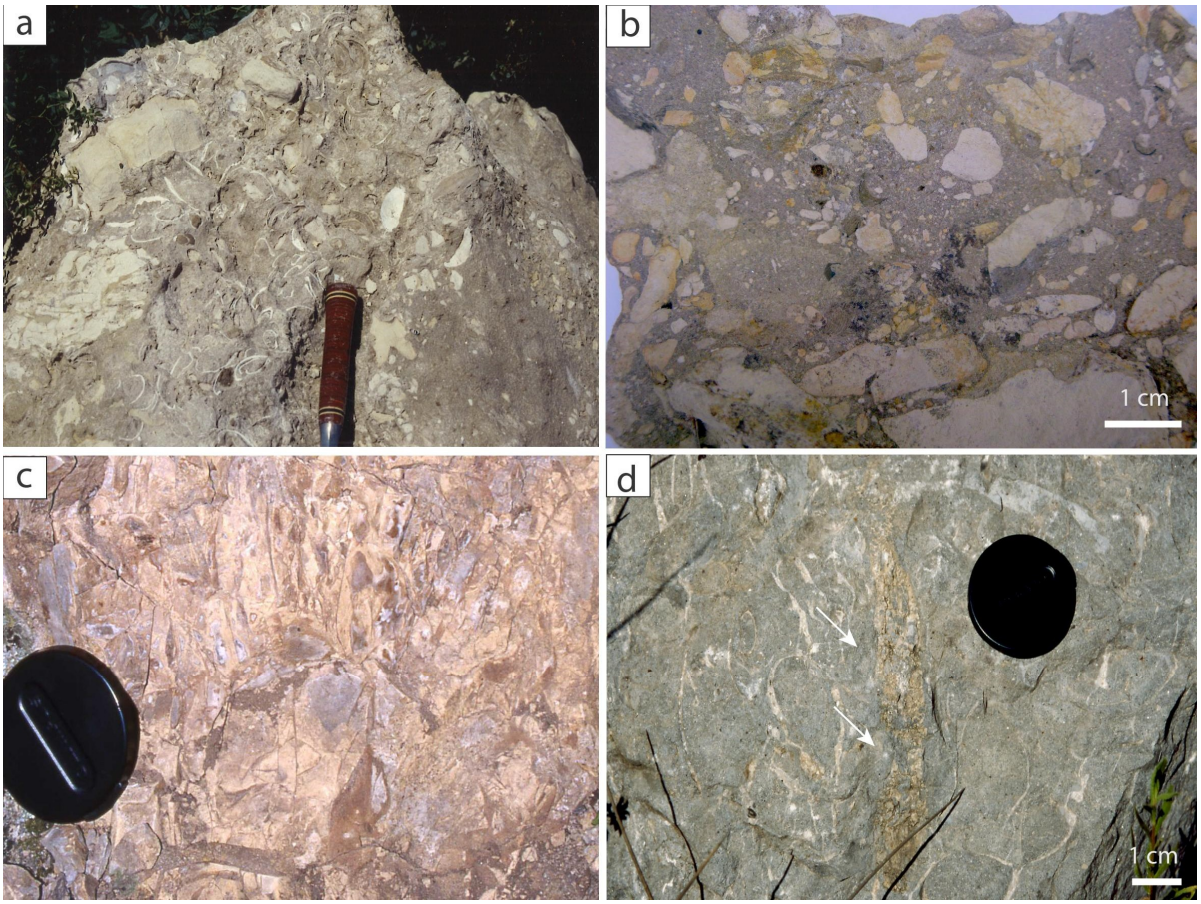

Figure 5. Examples of fluid-induced breccias: (**a**) Polygenic breccias with abundant disarticulated shells (COL outcrop in Figure 1). (**b**) Polygenic breccias with clasts floating in a micritic matrix (SV outcrop in Figure 1). (**c**) Carbonate monogenic breccia (CO outcrop in Figure 1). (**d**) Network of veins and a large conduit (arrows) filled with coarse sediments and carbonate cement (DE outcrop in Figure 1).

Stable C and O isotopic composition—Table 1 reports isotopic data for 160 carbonate samples collected in 12 outcrops. The examined seep-carbonates are mainly constituted of low-Mg calcite and minor aragonite and dolomite. They are typically depleted in $\delta^{13}C$ with values around −30‰ (Table 1). Values more negative than −50‰ occur in three outcrops (MP, LL, COL), with the most negative value is −56.2‰ (COL). Most samples display positive $\delta^{18}O$ values (up to 6.0‰), enriched respect to the carbonate fraction of surrounding sediments, that is generally around −1‰ [58,60]. The $\delta^{13}C$ depletion and ^{18}O enrichment reach the maximum values in clathrite-like textures, in particular from brecciated structures and conduit-rich facies.

Sediment instability in enclosing sediments related to fluid expulsion processes—Seep-carbonates are hosted in fine-grained deposits that in many cases show soft-sediment deformation structures, related to fluid expulsion (Figure 6a,b). In wedge-top outcrops (MSS), seep-carbonates are associated to chaotic deposits formed by the ascent of mud diapirs. In the foredeep, fluid-expulsion structures in host sediment adjacent to seep-carbonates include neptunian dikes and injection structures, chimneys and conduits filled by coarse deposits, cylindrical and ellipsoidal concretions, brecciated and septaria-like concretions made up of ^{13}C-depleted carbonate (Figure 6d). In the slope setting, slumps and slides have been frequently observed (MP). In many outcrops, fluidized resedimented arenites and debris flow are cemented by $\delta^{13}C$ depleted micrite (Figure 6c).

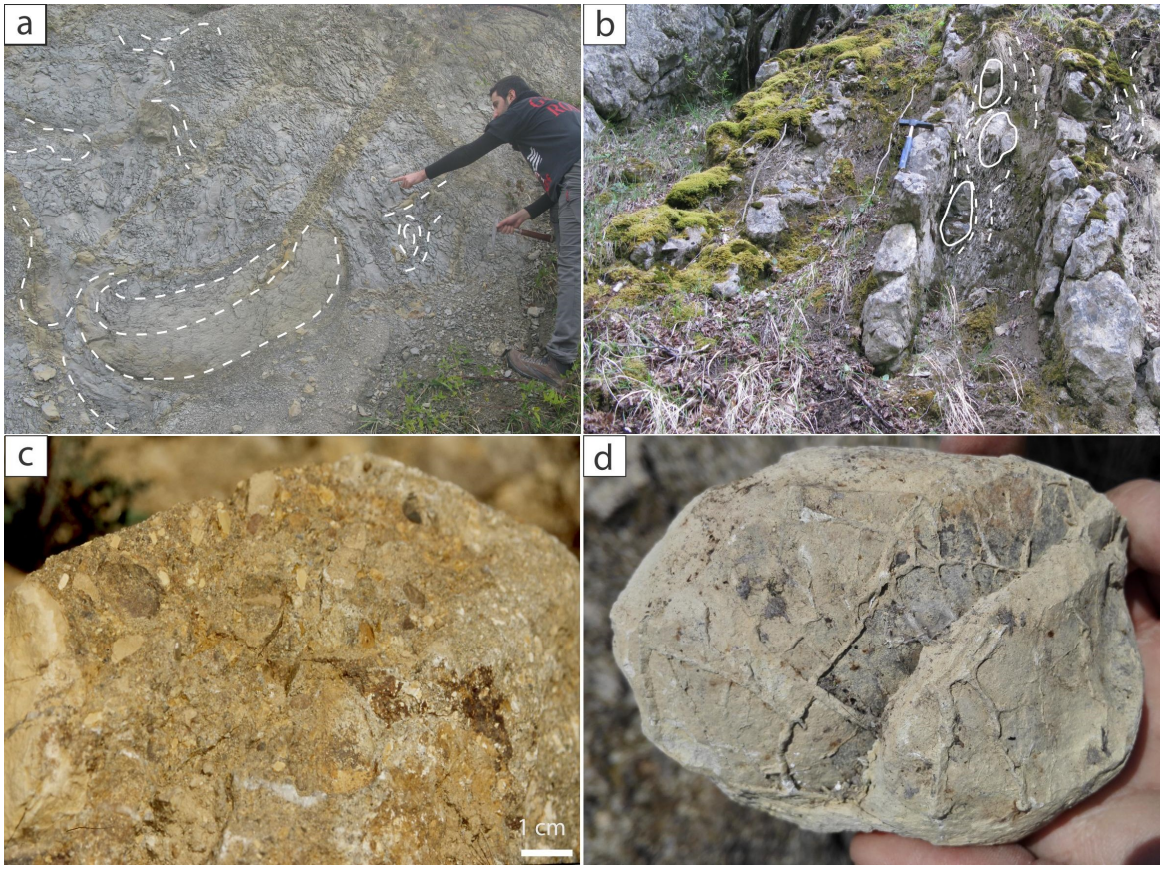

Figure 6. Examples of fluid expulsion structures: (**a**,**b**) Soft-sediment deformation structures and disrupted strata in host sediment in proximity of the seep carbonate body (COR outcrop in Figure 1). (**c**) Debris flow deposits cemented by ^{13}C-depleted micrite (DE outcrop of Figure 1). (**d**) Septaria-like concretion made up of depleted methane-derived carbonates (BU outcrop of Figure 1).

4.1. Dating of Seep Carbonate Outcrops

The biostratigraphy of the examined outcrops results from new analyses on nannofossil assemblages and from previous studies based on both nannofossils and foraminifera (Figure 7), carried out on the fine-grained hosting sediment. The examined sediments are distributed from the Langhian up to the early Messinian. In detail, two outcrops in the foredeep (CA, COR) are referred to the Langhian (nannofossil subzone MNN5a) in agreement with previous studies [51,60]. Based on nannofossil biostratigraphy, most of the seep outcrops (MMS, PC, COL, DE) indicate a Serravallian age. The CM and SAB outcrops provided similar ages, confirming previous analyses obtained with foraminifera [59]. Other seep-carbonate outcrops are referred to the early Tortonian; more in detail, SV correspond to the zone MNN8 and CB outcrop indicates subzone MNN8b and zone MNN9. Nannofossil assemblage in LL outcrop indicates the late Tortonian, whereas MP outcrop points to an age comprised between the late Tortonian and the early Messinian based on previous foraminifera biostratigraphy [53].

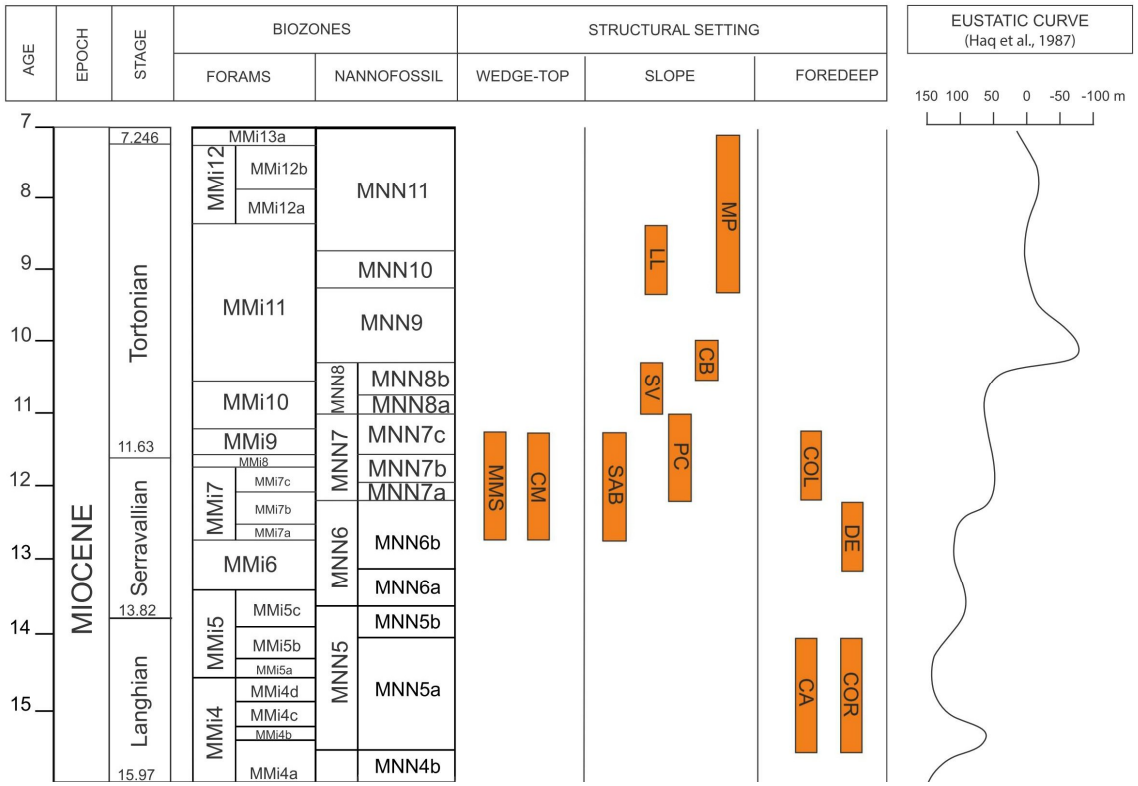

Figure 7. Biostratigraphic scheme, based on nannofossil and foraminifera assemblages, indicating the Miocene biozones and the stratigraphic distribution of the examined outcrops. For the full name of the outcrops refer to Figure 1. The third-order eustatic curve is reported to show a possible correlation between the development of seepage systems and low stands.

5. Discussion

We report several features in fossil seep-carbonates of the northern Apennines that can be related to the occurrence of paleo-gas hydrates. Some of these are similar to those described from present-day settings where gas hydrates have been mapped or directly observed on the seafloor, therefore their identification in the sedimentary record provides a quite robust evidence. The vacuolar, spongy and vuggy-like fabrics in the examined Apenninic carbonates are interpreted as voids and pores previously occupied by solid substances (possibly crystallization of gas hydrates at the rim of bubbles trapped in the sediment) [18] preserved by the precipitation of methane-derived carbonates. Monogenic breccias are made up of very angular micritic clasts of the previously precipitated carbonate crusts and may represent collapse breccias resulting from the rapid destabilization of gas hydrates within the sediment pore space [27]. Similar fabrics have been reported in seep-carbonates of the Hydrate Ridge [18] and in the Oligocene seep-carbonates of the Carpathians [42]. Polygenic breccias include exotic material derived from the underlying formations and could be related to rapid ascent of fluids released by gas hydrate destabilization: Similar structures are also described in carbonates associated to gas hydrates from the Hydrate Ridge (intraformational breccias) [18]. Fluid overpressures, as expected from the rapid decomposition of hydrates, can also result in the opening of fractures and injection of fluidized sediments [63–65] as shown in the dense and intricate network of non-systematic carbonate-filled veins and microfractures, irregularly connected to larger conduits, in the studied seep-carbonates. Layered carbonate facies show a zebra-like appearance due to the alternation of thin micrite and sparry calcite layers. This texture likely resulted from carbonate precipitation in contact with pure gas hydrate layers roughly oriented parallel to the bedding surfaces of the host sediments, as reported from present-day sediments at Hydrate Ridge, offshore Oregon [18].

Other markers are more uncertain, as the large dimension and volumes of carbonate bodies hardly explainable as originated by local anaerobic degradation of organic matter and more likely are indicative of abundant methane supply by destabilization of gas hydrates [56]. Moreover, according to various studies, fluid circulation for gas hydrate destabilization may trigger soft-sediment deformation and mass-wasting processes responsible for the emplacement of chaotic deposits [5,13]. Gas hydrates may act as cement, particularly in fine-grained deposits, improving cohesion and stability of paleo-slopes; conversely, their rapid decomposition increases sediment pore-pressure and favours sediment mobilization at all scales. Examined seep carbonate in the northern Apennines are sometimes associated with slumps, slides and resedimented arenites and debris flow, cemented or encrusted by micrite with depleted $\delta^{13}C$ and positive $\delta^{18}O$. In wedge-top outcrops, seep-carbonates are associated to chaotic deposits formed by the ascent of a mud diapir [49].

The oxygen isotopic composition of methane-derived carbonates provides important information on fluid sources and processes occurring within the sediments [27,56]. The ultimate $\delta^{18}O$ value recorded by authigenic carbonates is controlled by several factors, that is, the temperature of formation, the $\delta^{18}O$ composition of the precipitating fluid, the mineralogy and the pH of the solution [66–70]. Heavy $\delta^{18}O$ values (>+3.4‰ up to 14.8‰) [18,71] in methane-derived carbonates have been reported in gas hydrate-bearing sediments worldwide (Hydrate Ridge, Gulf of Mexico). Heaviest oxygen isotopic values in the examined seep-carbonates are around +5‰ and +6‰ (Table 1). Based on these $\delta^{18}O$ values, the temperature of formation of examined carbonates has been calculated applying the equation by [72] and assuming an original aragonitic mineralogy and pore fluid composition of 0‰ versus SMOW (average modern seawater). The resulting temperatures are below 0 °C which are clearly unrealistic. Therefore a contribution of isotopically heavier fluids has to be assumed: a possible influence of gas hydrate decomposition [27] or a contribution from deep-sourced fluids recording the dehydration of clay minerals [73]. We exclude the clay dehydration process, as the depth to the detachment surface under the foredeep deposits during the Miocene did not probably exceed 3 km [53], which is not sufficient to make the clay dehydration process a significant controlling factor on the oxygen isotopic composition of the carbonates [73]. We suggest that gas hydrate decomposition could be the main source at least for the heaviest $\delta^{18}O$ values in our study. In order to validate this hypothesis, we discuss the gas hydrate stability in the Apennines during the Miocene.

Gas Hydrate Stability along the Northern Apennine Margin during the Miocene

The stability of gas hydrates within the sediments depends on many factors such as temperature, pressure, gas composition and saturation, as well as pore-water composition (e.g., salinity) [27]. All these parameters are used to construct the stability curve for a specific gas hydrate structure. To calculate the vertical extent of the gas hydrate stability zone (GHSZ) we need to know the temperature profile in the water column and local geothermal gradient. The true depth interval in which hydrate potentially form within the sediments, called gas hydrate occurrence zone (GHOZ), is defined by the interceptions of the phase boundary curve with the seafloor and with the geothermal gradient (Figure 8) [74]. In order to reconstruct the gas hydrates stability in a fossil environment at a specific depth, we need to consider the bottom water temperature to calculate the GHOZ. In this way, we avoid introducing errors related to uncertainties on the oceanographic conditions due to paucity of data.

Paleobathimetric estimates of middle Miocene seep-carbonates in the inner foredeep by [75] and more recently by [57], place the seepage systems at the average depth of ~1000 m and we used this value as representative of the seafloor depth in our reconstruction (Figure 8). We calculated the stability field of pure methane hydrates (crystal structure I) [27] in the Miocene along the northern Apennine margin, since this methane hydrate structure is the most frequently observed along modern continental margins. We considered two different hypotheses of temperatures of bottom water, as reported by various authors for the Mediterranean region during the Miocene and a normal geothermal gradient of 30 °C/km. The value of 4 °C has been utilized by [48] for calculating the gas hydrate stability in the

lower Messinian sediments of the Tertiary Piedmont Basin (northern Italy). The authors extrapolated that value by applying an exponential curve decreasing from the Messinian sea surface temperature of 18 °C [76] until reaching the depth of 1000 m. By using 4 °C as minimum bottom water temperature and assuming modern-day Mediterranean salinity (3.8%) [77] we obtained a GHOZ of ~400 m for the Apennine setting (Figure 8). We then considered the bottom temperature of 11 °C as the highest value allowing a potential occurrence of gas hydrates within the sediments and consistent with a GHOZ of few tens of meters (Figure 8). A similar value of bottom water temperature (12–13 °C) has been also used by [41] to demonstrate that gas hydrates were stable at 1000 m water depth in the Western Mediterranean during the upper Miocene. Considering the paleobathimetry of our seepage systems and the expected depth of the thermocline located between 500 and 1000 m, the bottom temperature reported by [78] during the Middle Miocene Climatic Optimum (~15 °C at 500 m depth) would support the value of about 10 °C obtained in our model. Therefore, it is conceivable to use this latter value for the calculation of paleo-gas hydrates stability zones in the Miocene, indicating the potential occurrence of shallow gas hydrates.

The chronostratigraphic distribution of examined outcrops (Figure 7) shows that they are roughly concentrated in three main intervals: in the Langhian (MNN5a), in the late Serravallian-early Tortonian (MNN6b-MNN7) and the late Tortonian-early Messinian (MNN10-MNN11). When comparing seep distributions with 3rd order eustatic curves of [79], they approximately seem to match phases of sea-level lowering. However, in the studied cases, we are aware that the biostratigraphic resolution is conditioned by the duration of the biozone, that could be longer than the seepage activity. Some authors investigated the correlation between seep-carbonate precipitation and sea-level changes and proposed the correspondence of seep-carbonates with sea-level lowering [9,15,80]. A drop in the hydraulic pressure on the plumbing system during sea-level lowering would shift the bottom of the gas hydrate stability zone into shallower depths, inducing gas-hydrate destabilization [27]. Specific paleoclimatic reconstructions for the Miocene of the western Mediterranean will provide more accurate estimations.

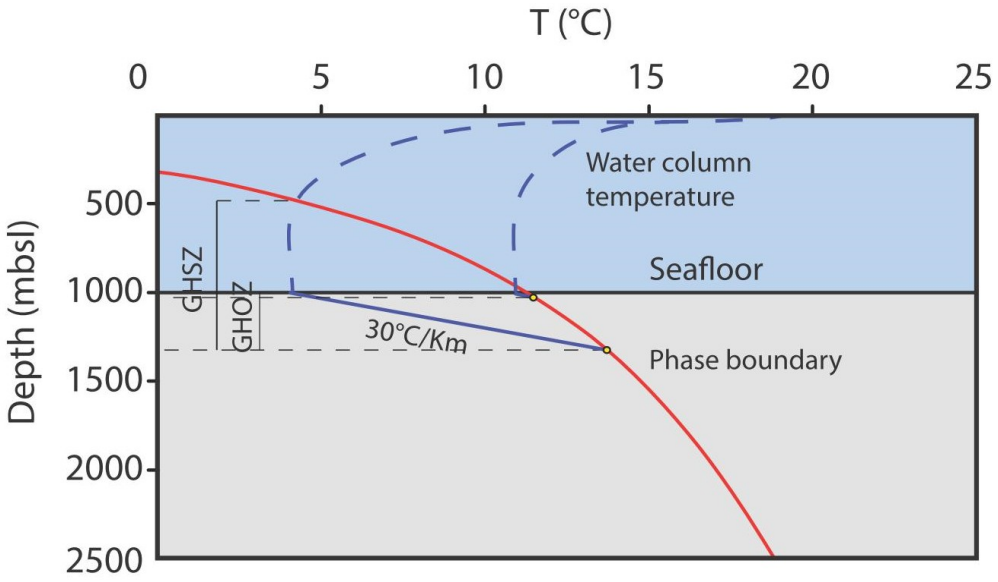

Figure 8. Evaluation of the gas hydrate stability along the northern Apennines in the Miocene, based on the assumptions reported in the text. For bottom water temperature of 4 °C, gas hydrates would be stable for 400 m below the seafloor. The value of 11 °C represents the highest temperature allowing the occurrence of gas hydrates in the upper tens of meters of sediments. Water column profiles were drawn following [48].

6. Conclusions

We document the occurrence of clathrite-like features in Miocene seep-carbonates from different structural settings of the Apennine wedge-foredeep system and discuss their possible relationships with gas hydrate dissociation.

Vuggy fabrics are interpreted as related to voids and pores previously occupied by gas hydrates dispersed in the sediment, preserved by the precipitation of methane-derived carbonates. It is suggested that monogenic and polygenic breccias could be related to rapid ascent of bubbles and growing gas hydrate layers that caused sediment brecciation. Fluid overpressures could result in the opening of fractures and injection of fluidized sediments. We also considered dimension and volumes of carbonate bodies, as well as sedimentary instability in host deposits, as possible indicator of abundant and prolonged methane supply by destabilization of gas hydrates.

We report heavy oxygen isotopic values up to +6‰ in the examined seep-carbonates and propose a contribution of isotopically heavier fluids released by gas hydrate decomposition.

Based on the calculation of gas hydrate stability zone for the selected settings, we suggest a potential occurrence of shallow gas hydrates within the sediments in the upper few tens of meters.

Supplementary Materials: The following are available online at http://www.mdpi.com/2076-3263/9/3/134/s1, S1: Full isotopic data.

Author Contributions: The authors contributed equally to this work.

Funding: This research was funded by the International Association of Sedimentologists, IAS Post-Graduate Grant 2nd session 2017, and by the University of Modena and Reggio Emilia PhD student research grant.

Acknowledgments: We are indebted to two anonymous Reviewers for helpful comments and suggestions.

Conflicts of Interest: The authors declare no conflict of interest.

References

1. Archer, D. Methane hydrate stability and anthropogenic climate change. *Biogeosciences* **2007**, *4*, 993–1057. [CrossRef]
2. Maslin, M.; Owen, M.; Betts, R.; Simon, D.; Dunkley Jones, T.; Ridgwell, A. Gas hydrates: Past and future geohazard? *Philos. Trans. R. Soc. A* **2010**, *368*, 2369–2393. [CrossRef] [PubMed]
3. Plaza-Faverola, A.; Klaeschen, D.; Barnes, P.; Pecher, I.; Henrys, S.; Mountjoy, J. Evolution of fluid expulsion and concentrated hydrate zones across the southern Hikurangi subduction margin, New Zealand: An analysis from depth migrated seismic data. *Geochem. Geophys. Geosyst.* **2012**, *13*. [CrossRef]
4. Ruppel, C.D.; Kessler, J.D. The interaction of climate change and methane hydrates. *Rev. Geophys.* **2017**, *55*, 126–168. [CrossRef]
5. Paull, C.K.; Buelow, W.J.; Ussler, W., III; Borowski, W.S. Increased continental-margin slumping frequency during sea-level lowstands above gas hydrate-bearing sediments. *Geology* **1996**, *24*, 143–146. [CrossRef]
6. Collett, T.S. Energy resource potential of natural gas hydrates. *AAPG Bull.* **2002**, *86*, 1971–1992.
7. Matsumoto, R.; Freire, A.F.M.; Machiyama, H.; Satoh, M.; Hiruta, A. Low velocity anomaly of gas hydrate bearing silty and clayey sediments, Joetsu Basin, Eastern Margin of Japan Sea. *AOGS* **2009**, *4*, 529–543.
8. Freire, A.F.M.; De Matos Maia Lete, C.; De Oliveira, F.M.; Guimaraes, M.F.; Da Silva Milhomen, P.; Pietzsch, R.; D'Avila, R.S.F. Fluid escape structures as possible indicators of past gas hydrate dissociation during the deposition of the Barremian sediments in the Reconcavo Basin, NE, Brasil. *Braz. J. Geol.* **2017**, *47*, 79–93. [CrossRef]
9. Haq, B.U. Natural gas hydrates: Searching for the long-term climatic and slope-stability records. In *Gas Hydrates: Relevance to World Margin Stability and Climate Change*; Henriet, J.P., Mienert, J., Eds.; Geological Society: London, UK, 1998; Volume 137, pp. 303–318.
10. Henriet, J.P.; Mienert, J. *Gas Hydrates—Relevance to World Margin Stability and Climatic Change*; Geological Society: London, UK, 1998; Volume 137, pp. 1–338.
11. Vogt, P.R.; Jung, W.Y. Holocene mass wasting on upper non-Polar continental slopes- due to post Glacial ocean warming and hydrate disssociation? *Geophys. Res. Lett.* **2002**, *29*, 1341–1348. [CrossRef]

12. Sultan, N.; Cochonat, P.; Foucher, J.P.; Mienert, J. Effect of gas hydrates melting on seafloor slope instability. *Mar. Geol.* **2004**, *213*, 379–401. [CrossRef]
13. Handwerger, A.L.; Rempel, A.W.; Skarbek, R.M. Submarine landslides triggered by destabilization of high-saturation hydrate anomalies. *Geochem. Geophys. Geosyst.* **2017**, *18*, 2429–2445. [CrossRef]
14. Pierre, C.; Fouquet, Y. Authigenic carbonates from methane seeps of the Congo deep-sea fan. *Geo-Mar. Lett.* **2007**, *27*, 249–257. [CrossRef]
15. Pierre, C.; Blanc-Valleron, M.; Demange, J.; Boudouma, O.; Foucher, J.P.; Pape, T.; Himnler, T.; Fekete, N.; Spiess, P. Authigenic carbonates from active methane seeps offshore southwest Africa. *Geo-Mar. Lett.* **2012**, *32*, 501–513. [CrossRef]
16. Kennett, J.P.; Fackler-Adams, B.N. Relationship of clathrate instability to sediment deformation in the upper Neogene of California. *Geology* **2000**, *28*, 215–218. [CrossRef]
17. Aloisi, G.; Pierre, C.; Rouchy, J.M.; Foucher, J.P.; Woodside, J.; Medinaut Scientific-Party. Methane-related authigenic carbonates of eastern Mediterranean Sea mud volcanoes and their possible relation to gas hydrate destabilisation. *Earth Planet. Sci. Lett.* **2000**, *184*, 321–338. [CrossRef]
18. Greinert, J.; Bohrmann, G.; Suess, E. Gas hydrate associated carbonates and methane venting at Hydrate Ridge: Classification, distribution and origin of authigenic lithologies. In *Natural Gas Hydrates: Occurrence, Distribution and Detection*; Geophysical Monograph Series; Paull, C.K., Dillon, W.P., Eds.; American Geophysical Union: Washington, DC, USA, 2001; Volume 124, pp. 99–113.
19. Sassen, R.; Roberts, H.H.; Carney, R.; Milkov, A.; DeFreitas, D.A.; Lanoil, B.; Zhang, C.L. Free hydrocarbon gas, gas hydrate and authigenic minerals in chemosynthetic communities of the northern Gulf of Mexico continental slope: Relation to microbial process. *Chem. Geol.* **2004**, *205*, 195–217. [CrossRef]
20. Mazzini, A.; Svensen, H.; Hovland, M.; Planke, S. Comparison and implications from strikingly different authigenic carbonates in a Nyegga complex pockmark, G11, Norwegian Sea. *Mar. Geol.* **2006**, *231*, 89–102. [CrossRef]
21. Ho, S.A.; Cartwright, J.A.; Imbert, P. Vertical evolution of fluid venting structures in relation to gas flux, in the Neogene-Quaternary of the Lower Congo Basin, Offshore Angola. *Mar. Geol.* **2012**, *332–334*, 40–55. [CrossRef]
22. Suess, E. Marine cold seeps and their manifestations: Geological control, biogeochemical criteria and environmental conditions. *Int. J. Earth Sci.* **2014**, *103*, 1889–1916. [CrossRef]
23. Smith, J.P.; Coffin, R.B. Methane-flux and authigenic carbonate in shallow sediments overlying methane hydrate bearing strata in Alaminos Canyon, Gulf of Mexico. *Energies* **2014**, *7*, 6118–6141. [CrossRef]
24. Bohrmann, G.; Heeschen, K.; Jung, C.; Weinrebe, W.; Baranov, B.; Cailleau, B.; Heath, R.; Huhnerbach, V.; Hort, M.; Masson, D.; et al. Widespread fluid expulsion along the seafloor of the Costa Rica convergent margin. *Terra Nova* **2002**, *14*, 69–79. [CrossRef]
25. Teichert, B.M.A.; Gussone, N.; Eisenhauer, A.; Bohrmann, G. Clathrites: Archives of near-seafloor pore-fluid evolution ($\delta^{44/40}$Ca, δ^{13}C, δ^{18}O) in gas hydrate environments. *Geology* **2005**, *33*, 213–216. [CrossRef]
26. Abegg, F.; Bohrmann, G.; Freitag, J.; Kuhs, W. Fabric of gas hydrate in sediments from Hydrate Ridge-results from ODP Leg 204 samples. *Geo-Mar. Lett.* **2007**, *27*, 269–277. [CrossRef]
27. Bohrmann, G.; Torres, M.E. Gas hydrates in marine sediments. In *Marine Geochemistry*; Schulz, H.D., Zabel, M., Eds.; Springer: Berlin, Germany, 2006; pp. 481–512.
28. Tong, H.; Feng, D.; Cheng, H.; Yang, S.; Wang, H.; Min, A.G.; Edwards, R.L.; Chen, Z.; Chen, D. Authigenic carbonates from seeps on the northern continental slope of the South China Sea: New insights into fluid sources and geochronology. *Mar. Pet. Geol.* **2013**, *13*, 260–271. [CrossRef]
29. Han, X.; Suess, E.; Liebetrau, V.; Eisenhauer, A.; Huang, Y. Past methane release events and environmental conditions at the upper continental slope of the South China Sea: Constraints by seep carbonates. *Int. J. Earth Sci.* **2014**, *103*, 1873–1887. [CrossRef]
30. Loyd, S.J.; Sample, J.; Tripati, R.E.; Defliese, W.F.; Brooks, K.; Hovland, M.; Torres, M.; Marlow, J.; Hancock, L.G.; Martin, R.; et al. Methane seep carbonates yield clumped isotope signatures out of equilibrium with formation temperatures. *Nat. Commun.* **2016**, *7*, 12274. [CrossRef]
31. Naehr, T.H.; Rodriguez, N.M.; Bohrmann, G.; Paull, C.K.; Botz, R. Methane derived authigenic carbonates associated with gas hydrate decomposition and fluid venting above the Blake Ridge Diapir. *Proc. ODP Sci. Results* **2000**, *164*, 285–300.

32. Matsumoto, R.; Borowski, W.S. Gas-hydrate estimate from newly determined oxygen isotopic fractionaction ($\alpha_{GH\text{-}IW}$) and ^{18}O anomalies of the interstitial waters. Leg 164, Blake Ridge. *Proc. ODP Sci. Results* **2000**, *164*, 59–66.
33. Heeschen, K.U.; Haeckel, M.; Klaucke, I.; Ivanov, M.K.; Bohrmann, G. Quantifying in situ gas hydrates at active seep sites in the eastern Blake Sea using pressure coring technique. *Biogeosciences* **2011**, *8*, 3555–3565. [CrossRef]
34. Larrasoaña, J.C.; Roberts, A.P.; Musgrave, R.J.; Gràcia, E.; Piñero, E.; Vega, M.; Martínez-Ruiz, F. Diagenetic formation of greigite and pyrrhotite in gas hydrate marine sedimentary systems. *Earth Planet. Sci. Lett.* **2007**, *261*, 350–366. [CrossRef]
35. Wendel, J. Ancient methane seeps tell tale of sudden warming. *EOS* **2017**, *98*. [CrossRef]
36. Hesselbo, S.P.; Grocke, D.R.; Jenkins, H.C.; Bjerrum, C.J.; Farrimond, P.; Bell, H.S.M.; Green, O.R. Massive dissociation of gas hydrate during a Jurassic oceanic anoxic event. *Nature* **2000**, *406*, 392–395. [CrossRef] [PubMed]
37. Padden, M.; Weissert, H.; De Rafelis, M. Evidence for Late Jurassic release of methane from gas hydrate. *Geology* **2001**, *29*, 223–226. [CrossRef]
38. Kennedy, M.J.; Christie-Blick, N.; Sohl, L.E. Are Proterozoic cap carbonates and isotopic excursions a record of gas hydrate destabilization following Earth's coldest intervals? *Geology* **2001**, *29*, 443–446. [CrossRef]
39. Krause, F.F. Genesis and geometry of the Meiklejohn Peak lime mud-mound, Bare Mountain Quadrangle, Nevada, USA. Ordovician limestone with submarine frost heave structures—A possible response to gas clathrate hydrate evolution. *Sediment. Geol.* **2001**, *145*, 189–213. [CrossRef]
40. Pierre, C.; Rouchy, G.M.; Blanc-Valleron, M.M. Gas hydrate dissociation in the Lorca Basin (SE Spain) during the Mediterranean Messinian salinity crisis. *Sediment. Geol.* **2002**, *147*, 247–252. [CrossRef]
41. Pierre, C.; Rouchy, J.M. Isotopic compositions of diagenetic dolomites in the Tortonian marls of the western Mediterranean margins: Evidence of past gas hydrate formation and dissociation. *Chem. Geol.* **2004**, *205*, 469–484. [CrossRef]
42. Bojanowski, M.J.; Bagiński, B.; Guillermier, C.; Franchi, I.A. Carbon and oxygen isotope analysis of hydrate-associated Oligocene authigenic carbonates using NanoSIMS and IRMS. *Chem. Geol.* **2015**, *416*, 51–64. [CrossRef]
43. Himmler, T.; Freiwald, A.; Stollhofen, H.; Peckmann, J. Late Carboniferous hydrocarbon-seep carbonates from the glaciomarine Dwyka Group, southern Namibia. *Palaeogeogr. Palaeoclimatol. Palaeoecol.* **2008**, *257*, 185–197. [CrossRef]
44. Wang, J.; Jiang, G.; Xiao, S.; Li, Q.; Wei, Q. Carbon isotope evidence for widespread methane seeps in the ca.635 Ma Doushantuo cap carbonate in south China. *Geology* **2008**, *36*, 347–350. [CrossRef]
45. Nyman, S.L.; Nelson, C.S.; Campbell, K.A. Miocene tubular concretions in East Coast Basin, New Zealand: Analogue for subsurface plumbing of cold seeps. *Mar. Geol.* **2010**, *272*, 319–336. [CrossRef]
46. Iadanza, A.; Sanpalmieri, G.; Cipollari, P.; Mola, M.; Cosentino, D. The "Brecciated Limestones" of Maiella, Italy: Rheological implications of hydrocarbon-charged fluid migration in the Messinian Mediterranean Basin. *Palaeogeogr. Palaeoclimatol. Palaeoecol.* **2013**, *390*, 130–147. [CrossRef]
47. Peckmann, J.; Thiel, V. Carbon cycling at ancient methane-seeps. *Chem. Geol.* **2004**, *205*, 443–467. [CrossRef]
48. Dela Pierre, F.; Martire, L.; Natalicchio, M.; Clari, P.; Petrea, C. Authigenic carbonates in Upper Miocene sediments of the Tertiary Piedmont Basin (NW Italy): Vestiges of an ancient gas hydrate stability zone? *GSA Bull.* **2010**, *122*, 994–1010. [CrossRef]
49. Conti, S.; Fontana, D.; Lucente, C.C.; Pini, G.A. Relationships between seep-carbonates, mud volcanism and basin geometry in the Late Miocene of the northern Apennines of Italy: The Montardone mélange. *Int. J. Earth Sci.* **2014**, *103*, 281–295. [CrossRef]
50. Conti, S.; Fioroni, C.; Fontana, D. Correlating shelf carbonate evolutive phases with fluid expulsion episodes in the foredeep (Miocene, northern Apennines, Italy). *Mar. Pet. Geol.* **2017**, *79*, 351–359. [CrossRef]
51. Argentino, C.; Conti, S.; Crutchley, G.J.; Fioroni, C.; Fontana, D.; Johnson, J.E. Methane-derived authigenic carbonates on accretionary ridges: Miocene case studies in the northern Apennines (Italy) compared with modern submarine counterparts. *Mar. Pet. Geol.* **2019**, *102*, 860–872. [CrossRef]
52. Conti, S.; Fioroni, C.; Fontana, D.; Grillenzoni, C. Depositional history of the Epiligurian wedge-top basin in the Val Marecchia area (northern Apennines, Italy): A revision of the Burdigalian-Tortonian succession. *Ital. J. Geosci.* **2016**, *135*, 324–335. [CrossRef]

53. Conti, S.; Fontana, D.; Mecozzi, S.; Panieri, G.; Pini, G.A. Late Miocene seep-carbonates and fluid migration on top of the Montepetra intrabasinal high (Northern Apennines, Italy): Relations with synsedimentary folding. *Sediment. Geol.* **2010**, *231*, 41–54. [CrossRef]
54. Tinterri, R.; Magalhaes, P.M. Synsedimentary structural control on foredeep turbidites: An example from Miocene Marnoso-arenacea Formation, Northern Apennines, Italy. *Mar. Pet. Geol.* **2011**, *28*, 629–657. [CrossRef]
55. Ricci Lucchi, F. The Oligocene to Recent Foreland basins of the Northern Apennines. In *Foreland Basins*; Allen, P.A., Homewood, P., Eds.; The International Association of Sedimentologists: Gent, Belgium, 1986; Volume 8, pp. 103–139.
56. Campbell, K.A. Hydrocarbon seep and hydrothermal vent paleoenvironments and paleontology: Past developments and future research directions. *Paleogeogr. Paleoclimatol. Paleoecol.* **2006**, *232*, 362–407. [CrossRef]
57. Grillenzoni, C.; Monegatti, P.; Turco, E.; Conti, S.; Fioroni, C.; Fontana, D.; Salocchi, A.C. Paleoenvironmental evolution in a high-stressed cold-seep system (Vicchio Marls, Miocene, northern Apennines, Italy). *Palaeogeogr. Palaeoclimatol. Palaeoecol.* **2017**, *487*, 37–50. [CrossRef]
58. Terzi, C.; Lucchi, F.R.; Vai, G.B.; Aharon, P. Petrography and stable isotope aspects of cold-vent activity imprinted on Miocene-age "calcari aLucina" from Tuscan and Romagna Apennines, Italy. *Geo-Mar. Lett.* **1994**, *14*, 177–184. [CrossRef]
59. Conti, S.; Fontana, D.; Gubertini, A.; Sighinolfi, G.; Tateo, F.; Fioroni, C.; Fregni, P. A multidisciplinary study of middle Miocene seep-carbonates from the northern Apennine foredeep (Italy). *Sediment. Geol.* **2004**, *169*, 1–19. [CrossRef]
60. Conti, S.; Fontana, D.; Lucente, C.C. Authigenic seep-carbonates cementing coarse-grained deposits in a fan-delta depositional system (middle Miocene, Marnoso-arenacea Formation, central Italy). *Sedimentology* **2008**, *55*, 471–486. [CrossRef]
61. Artoni, A.; Conti, S.; Turco, E.; Iaccarino, S. Tectonic and climatic control on deposition of seep-carbonates: The case of middle-late Miocene Salsomaggiore Ridge (Northern Apennines, Italy). *Rivista Italiana di Paleontologia e Stratigrafia* **2014**, *120*, 317–335.
62. Martire, L.; Natalicchio, M.; Petrea, C.C.; Cavagna, S.; Clari, P.; Pierre, F.D. Petrographic evidence of the past occurrence of gas hydrates in the Tertiary Piedmont Basin (NW Italy). *Geo-Mar. Lett.* **2010**, *30*, 461–476. [CrossRef]
63. Shanmugam, G. Global case studies of soft-sediment deformation structures (SSDS): Definitions, classifications, advances, origins and problems. *J. Palaeogeogr.* **2017**, *6*, 251–320. [CrossRef]
64. Schwartz, H.; Sample, J.; Weberling, K.D.; Minisini, D.; Moore, J.C. An ancient linked fluid migration system: Cold-seep deposits and sandstone intrusions in the Panoche Hills, California, USA. *Geo-Mar. Lett.* **2003**, *23*, 340–350. [CrossRef]
65. Mazzini, A. Mud volcanism: Processes and implications. *Mar. Pet. Geol.* **2009**, *26*, 1677–1680. [CrossRef]
66. Friedman, I.; O'Neil, J.R. Compilation of stable isotope fractionation: Factors of geochemical interest. In *Data of Geochemistry*, 6th ed.; Geological Survey Professional Paper; Fleischer, M., Ed.; USGS: Washington, DC, USA, 1977; pp. 1–12.
67. Tremaine, D.M.; Froelich, P.N.; Wang, Y. Speleothem calcite farmed in situ: Modern calibration of ^{18}O and ^{13}C paleoclimate proxies in a continuously-monitored natural cave system. *Geochim. Cosmochim. Acta* **2011**, *75*, 4929–4950. [CrossRef]
68. Tarutani, T.; Clayton, R.N.; Mayeda, T.K. The effect of polymorphism and Mg substitution on oxygen isotope fractionation between calcium carbonate and water. *Geochim. Cosmochim. Acta* **1969**, *33*, 987–996. [CrossRef]
69. Emrich, K.; Ehhalt, D.H.; Vogel, J.C. Carbon isotope fractionation during the precipitation of calcium carbonate. *Earth Planet. Sci. Lett.* **1970**, *8*, 363–371. [CrossRef]
70. Zeebe, R.E.; Wolf-Gladrow, D. *CO_2 in Seawater: Equilibrium, Kinetics, Isotopes*; Elsevier: Amsterdam, The Netherlands, 2001; 346p.
71. Feng, D.; Birgel, D.; Peckmann, J.; Roberts, H.H.; Joye, S.B.; Sassen, R.; Liu, X.L.; Hinrichs, K.U.; Chen, D. Time integrated variation of sources of fluids and seepage dynamics archived in authigenic carbonates from Gulf of Mexico Gas Hydrate Seafloor Observatory. *Chem. Geol.* **2014**, *385*, 129–139. [CrossRef]
72. Hudson, J.D.; Anderson, T.F. Ocean temperatures and isotopic compositions through time. *Earth Environ. Sci. Trans. R. Soc. Edinb.* **1989**, *80*, 183–192. [CrossRef]

73. Dählmann, A.; De Lange, G.J. Fluid–sediment interactions at Eastern Mediterranean mud volcanoes: A stable isotope study from ODP Leg 160. *Earth Planet. Sci. Lett.* **2003**, *212*, 377–391. [CrossRef]
74. Tréhu, A.M. Gas hydrates in marine sediments: Lessons from scientific ocean drilling. *Oceanography* **2006**, *19*, 124–142. [CrossRef]
75. Aharon, P.; Sen Gupta, B.K. Bathymetric reconstructions of the Miocene age "calcari a Lucina" (Northern Apennines, Italy) from oxigen isotopes and benthic foraminifera. *Geo-Mar. Lett.* **1994**, *14*, 219–230. [CrossRef]
76. Bosellini, F.R.; Perrin, C. Estimating Mediterranean Oligocene-Miocene sea-surface temperatures: An approach based on coral taxonomic richness. *Paleogeogr. Paleoclimatol. Paleoecol.* **2008**, *258*, 71–88. [CrossRef]
77. Wenzhöfer, F. *Short Cruise Report MERIAN MSM 13/4 HOMER Limassol-Limassol 21.11. 2009 14.12. 2009*; Max Planck Institut für Marine Mikrobiologie: Bremen, Germany, 2009.
78. Scheiner, F.; Holcová, K.; Milovský, R.; Kuhnert, H. Temperature and isotopic composition of seawater in the epicontinental sea (Central Paratethys) during the Middle Miocene Climate Transition based on Mg/Ca, $\delta^{18}O$ and $\delta^{13}C$ from foraminiferal tests. *Palaeogeogr. Palaeoclimatol. Palaeoecol.* **2018**, *495*, 60–71. [CrossRef]
79. Haq, B.U.; Hardenbol, J.A.N.; Vail, P.R. Chronology of fluctuating sea levels since the Triassic. *Science* **1987**, *235*, 1156–1167. [CrossRef] [PubMed]
80. Fontana, D.; Conti, S.; Grillenzoni, C.; Mecozzi, S.; Petrucci, F.; Turco, E. Evidence of climatic control on hydrocarbon seepage in the Miocene of the northern Apennines: The case study of the Vicchio Marls. *Mar. Pet. Geol.* **2013**, *48*, 90–99. [CrossRef]